KRONOS FUSION ENERGY

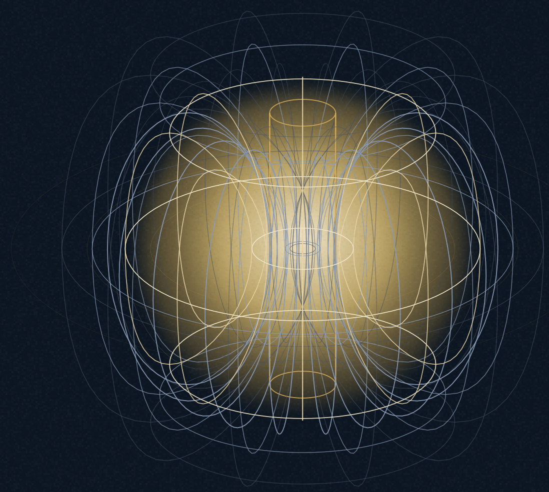

PAPER 2.34 · THE KRONOS 2026 SERIES

A Real-Time Tritium-Accountancy Twin for a Compact Spherical-Tokamak Breeder: In-Vessel Inventory, Retention, and Self-Sufficiency Bookkeeping

A deuterium–tritium breeder must know, at all times, where its tritium is: tritium is simultaneously the fuel, the product, and the principal radiological hazard, and it is mobile...

Read it live — 3-D model · physics validator · film series

BY P I FORD

2026 · EDITORIAL EDITION

THE OFFICIAL RECORD

What this document is, and how to read its numbers

This is a combined editorial. It gathers, in one volume, the two design studies Kronos Fusion Energy released in 2026 — a compact spherical-tokamak tritium/helium-3 breeder and a deuterium–helium-3 tandem-mirror generator — together with the intellectual-property estate, the people, and, in the internal edition, the full commercial case. The scientific text is the same text that appears in the arXiv preprints and the journal submissions; the editorial adds the apparatus a reader needs to hold the whole program at once, and nothing in the physics is altered to fit it.

THE HONESTY STANCE IS THE ASSET

Every headline quantity carries an **evidence class** — DERIVED RECOMPUTED MEASURED REQUIREMENT — and, where a number is a modelled extrapolation rather than a demonstrated value, it is labelled as such and its downside is shown next to it. Several quantities in the underlying corpus moved after first publication; where a value has been withdrawn or restated, the record says so plainly. This is deliberate: a diligence team will find the load-bearing assumptions, so the document surfaces them first.

TWO EDITIONS

This volume is issued in two editions. The **public edition** (light) carries the physics and the design only — no dollar, price, or per-kilogram figure appears anywhere in it. The **internal edition** (dark) adds the economics, the funding architecture, and the defense-commercial analysis, and is marked *Confidential* accordingly; it is not for public distribution. Where the commercial case rests on a modelled assumption rather than a demonstrated one, it is labelled as such and its downside is shown alongside it, on the same terms as the physics.

TITLE	The Kronos Fleet — Hyperion · Aegis · MetroVolt: A Combined Design & Commercialization Study
AUTHOR	Priyanca Ford, Founder & CEO, on behalf of Kronos Fusion Energy
EDITION	2026 Combined Editorial · first issue
COMPANION WORKS	The five-paper arXiv drop — (1) Breeder, (2) Burner, (3) REBCO magnet & tape, (4) Direct Energy Conversion, (5) AI/ML/Quantum control — with matching numbered Zenodo deposits, plus the IOP journal and IAEA-FEC submissions. Patents were filed before the drop.
NAMING	Hyperion = the breeder; Aegis (defense) and MetroVolt (data-center) = one generator in two housings. Internal mode letters (D1, L) do not appear on public surfaces.
STATUS	Conceptual design & simulation study. Nothing herein is a construction commitment.

HOW TO READ THIS VOLUME

The fleet at a glance, and the way its numbers are marked

This volume opens with *Orientation*, presents the five research papers as a bound sequence, and closes with the *Apparatus*. *Foundations* sets out the three general results both machines rest on. *Paper One* is the Hyperion breeder; *Paper Two* the Aegis / MetroVolt generator; *Papers Three, Four and Five* are the enabling science — high-field REBCO magnets and tape, direct energy conversion, and the AI / ML / quantum control stack. A *Digital Twin & 3-D Model* part follows, then the *Environmental* profile. The *Economics* and levelized cost and the *Business Case* and diligence record appear in the internal edition only; the *Simulations* proof record and the Apparatus — patent portfolio, team, limitations, and sources — close both editions.

THE FLEET AT A GLANCE

	HYPERION	AEGIS	METROVOLT
Role	Strategic-isotope foundry	Defense installation power	Campus power
Machine	**Spherical tokamak**	**Tandem mirror**	**Tandem mirror**
Fuel	Deuterium–tritium	Deuterium–helium-3	Deuterium–helium-3
Delivers	Tritium · ^{3}He · 14 MeV n	Resilient installation power	Firm campus power
Physics bar	**Fusion gain only**	Closure (gates named)	Closure + lunar ^{3}He
In the fleet	Breeds the fuel	Proves the generator	Commercial destination

HOW THE NUMBERS ARE MARKED

Every headline quantity carries an evidence class — DERIVED from first principles, RECOMPUTED from raw data, MEASURED in hardware, or a REQUIREMENT yet to be met. Financial figures carry a case label and are confined to the internal (confidential) edition. Values that moved after first publication are shown as withdrawn or restated rather than quietly changed. A capability you can evaluate is one whose limits are on the page.

ABSTRACT

A Real-Time Tritium-Accountancy Twin for a Compact Spherical-Tokamak Breeder: In-Vessel Inventory, Retention, and Self-Sufficiency Bookkeeping

A deuterium–tritium breeder must know, at all times, where its tritium is: tritium is simultaneously the fuel, the product, and the principal radiological hazard, and it is mobile — it permeates, it is trapped, and it is bred faster than it is burned. Closing the tritium balance in real time to safeguards tolerance therefore rests on two quantities the plant cannot measure directly and must compute: how much tritium is held inside the vessel wall, and how much is leaking through it. We fix both from a finite-element hydrogen-transport solve (FESTIM) of the actual first-wall stack of the Hyperion breeder — $0.5\,mm$ tungsten armour on $2\,mm$ Eurofer97-class steel — using a McNabb–Foster diffusion–trapping model with Sieverts chemical-potential continuity at the interface. The steady permeation loss is $5.16 \times 10^{14}\ \mathrm{T\,m^{-2}\,s^{-1}}$ ($\approx 0.082\,g\,\mathrm{T\,m^{-2}\,fpy^{-1}}$; 0.52–0.60% of the implanted flux, with $\sim 99.4\%$ re-emitted), it is diffusion-limited in the tungsten armour, temperature- independent, and exactly linear in wall load, and the finite-element flux reproduces the analytic two-layer series-resistance limit to seven significant figures. The retained in-wall inventory is strongly temperature- dependent, ranging from $8.8\,\mu g/m^2$ on the operating gradient ($800 \to 600\,K$) to $0.42\,mg/m^2$ in the cold $600\,K$ bound, and breakthrough is reached within 30–$190\,s$ of a burn start — a fast, well-posed state. Integrated over a $\sim 100\,m^2$ first wall the permeation term is ~ 8–$10\,g\,\mathrm{T\,fpy^{-1}}$, negligible against a per-unit breeding surplus of 1.62–$3.82\,kg\,\mathrm{T\,fpy^{-1}}$. On this measured budget we cast the accountancy problem as a state-estimation problem over the plant tritium balance, specify a maturity-gated accountancy twin — a real-time balance, an in-vessel inventory estimator, a lithium-6 tracker, and coupled corrosion and waste-classification monitors — and separate the tritium bred as product from the tritium held as holdup, so the books close simultaneously against the fuel cycle (which needs the surplus) and the safeguards frame (which needs the holdup bounded).

Open-access deposit (code & data, CC BY 4.0): DOI 10.5281/zenodo.22645876 · Zenodo community *kronos_fusion_energy*. Explore it live: interactive 3-D model · physics validator.

Keywords: tritium accountancy · in-vessel inventory · permeation · FESTIM · digital twin · self-sufficiency · safeguards · spherical-tokamak breeder

CONTENTS

Table of Contents

A Real-Time Tritium-Accountancy Twin for a Compact Spherical-Tokamak Breeder: In-Vessel Inventory, Retention, and Self-Sufficiency Bookkeeping 3
Introduction 6
Governing equations and the formal accountancy problem 8
Computational methodology: the GPU-HPC campaign 10
Results: the measured in-vessel tritium budget 12
The accountancy twin 19
Separating product from holdup 21
Discussion 22
Limitations 23
Conclusion 24
References 29
One programme, many papers 33

NOMENCLATURE

Symbols, units, and the names of things

Q	plasma (fusion) gain, P_{fus}/P_{aux}
Q_E	engineering gain, net electric out / recirculating in
H_{98}	confinement enhancement over the IPB98(y,2) scaling
Z_{eff}	effective ion charge
c_{ee}	electron–electron bremsstrahlung leading coefficient, 2.120022 (exact)
τ_E	energy confinement time
I_p	plasma current
R_0, a	major radius, minor radius
κ, δ	elongation, triangularity
β_N	normalized plasma beta (Troyon-normalized)
TBR	tritium breeding ratio
DEC	direct energy conversion
CF	plant capacity factor (availability)
FOAK / NOAK / BOAK	first / n^{th} / best of a kind
Hyperion	the ST breeder (internal: Mode D2)
Aegis	the generator, defense/installation housing (internal: Mode M)
MetroVolt	the generator, data-center housing (Mode M)

§ 1

Introduction

ACCOUNTANCY AS A FIRST-ORDER OPERATIONAL REQUIREMENT

In a deuterium–tritium (D–T) fusion breeder the tritium is not an inert working fluid. It is the fuel, the bred product, and the dominant radiological source term, and it is mobile on every timescale of interest: it is implanted into and re-emitted from plasma-facing surfaces, it diffuses and is trapped in the structure, it is bred in the blanket faster than it is burned, and it decays with a $12.32\,yr$ half-life into helium-3 [1]. Knowing *how much tritium is where*, continuously, and closing the balance to safeguards tolerance is therefore a first-order operational requirement, not a back-office audit. It is also the quantity on which the two headline claims of a breeder rest — that the plant is tritium self-sufficient with a bankable surplus [16,18,19], and that its mobile in-vessel inventory is bounded well below licensing limits [20].

Tritium accountancy in a fusion plant differs from fissile-material accountancy in a way that makes it harder, not easier: a large fraction of the tritium at any instant is not in a tank where it can be assayed but is distributed through the machine — implanted in walls, trapped at defects, dissolved in coolant, and resident in the breeder ceramic. Two of these terms cannot be measured directly at operating temperature and pressure and must instead be *computed* from transport physics and tracked by a model: the tritium held inside the vessel wall, and the tritium permeating through it into the structure and coolant. This paper fixes both from first principles for the Hyperion breeder and specifies the real-time twin that tracks them.

THE DESIGN POINT

Hyperion is a compact, negative-triangularity spherical tokamak (ST) operated as a strategic-materials breeder rather than a net-electric plant [2,3]. Its frozen design point is $Q = 3.076$, fusion power $P_{\text{fus}} = 85.04\,MW$, plasma current $I_p = 9.66\,MA$, negative triangularity $\delta = -0.30$, on-axis field $B_0 = 8\,T$, elongation $\kappa = 2.0$, major radius $R_0 = 1.20\,m$, aspect ratio $A = 2.5$, and a consumable centrepost at a peak field of $16.84\,T$. Negative triangularity is chosen for good confinement without an edge pressure pedestal [4,5]; the compactness that makes the ST an attractive volumetric neutron source also concentrates the fusion power, so the first-wall implantation flux — and hence the tritium the wall holds and passes — is set by a high, well-defined wall load. At $P_{\text{fus}} = 85.04\,MW$ the plant burns $4.769\,kg$ of tritium per full-power year (fpy), so a permeation loss measured in grams per fpy is a small but real term in a kilogram-scale ledger, and the held wall inventory is the state a safeguards estimator must follow.

PRIOR ART

The transport physics of hydrogen isotopes in tungsten and reduced-activation ferritic–martensitic (RAFM) steel is mature. Frauenfelder's diffusion and solubility data for hydrogen in tungsten [6] and the McNabb–Foster diffusion–trapping formalism [7] underpin essentially all first-wall retention modelling [9,10]; deuterium-retention measurements in tungsten established the intrinsic-trap populations used here [8], and permeation and trapping in Eurofer97 have been characterised over the relevant temperature window [11]. These data are now assembled into open finite-element transport codes — FESTIM, built on the FEniCS finite-element platform [12,13,14], and the INL systems code TMAP [15] — so that the retention and permeation of a specified plasma-facing stack are computable rather than assumed. On the systems side, the conditions for tritium self-sufficiency and the required start-up inventory have been analysed for DEMO-class plants [16,17,18,19], and the digital-twin formalism — a model of a specific asset, updated by that asset's data and used to predict and steer it [21] — has matured to the point where a real-time transport model can run inside the plant control cycle.

Within the Kronos series the surrounding fuel-cycle results are frozen. The tritium breeding ladder, per-unit inventory and fleet doubling path are established in the breeding-ladder study [doi:10.5281/zenodo.22645746; official page], the net-TBR case for multi-unit tritium export in the breeding-lever study [doi:10.5281/zenodo.22645706; official page], and the tritium safety and source-term case in the environmental study [doi:10.5281/zenodo.22645754; official page]. The permeation-barrier wall-chemistry choice that bounds the loss term is treated separately [doi:10.5281/zenodo.22645870; official page].

CONTRIBUTION

What is missing — and what this paper supplies — is the bridge from these computed transport numbers to a real-time accountancy state that closes the tritium books live. We contribute: (i) a formal statement of the plant tritium-balance and self-sufficiency problem, and of the in-wall transport that supplies its loss and holdup terms (§2); (ii) the finite-element formulation and its analytic verification, together with the NVIDIA GPU HPC campaign that produced the frozen result set (§3); (iii) the measured in-vessel tritium budget — permeation loss, retained inventory, its temperature dependence, and breakthrough time — with eight data figures traceable to frozen register serials (§4); (iv) the accountancy twin cast as a state-estimation problem, with its module set and pre-registered acceptance tests (§5); and (v) the explicit separation of bred product from structural holdup that lets one balance close against both the fuel cycle and the safeguards frame (§6). Every quantitative claim traces to a frozen result in the Kronos Physics De-Risking Register [31], and the governing serial (BR-L2-A25, FESTIM) is cited inline so each number is auditable. This work is the tritium instance of the four-coupled-twin control architecture [doi:10.5281/zenodo.22645805; official page] and shares its maturity-gated authority pattern.

§ 2

Governing equations and the formal accountancy problem

THE PLANT TRITIUM BALANCE

The quantity accountancy exists to track is the total mobile tritium inventory $I_T(t)$ of the plant. Its balance collects breeding, burn, radioactive decay, and processing/structural losses (BR-L1-A6, BR-L1-A8):

$$\frac{\mathrm{d}I_T}{\mathrm{d}t} = \dot{N}_{\text{bred}} - \dot{N}_{\text{burn}} - \lambda_T I_T - \dot{N}_{\text{loss}}, \qquad \lambda_T = \frac{\ln 2}{t_{1/2}}, \quad t_{1/2} = 12.32\,\text{yr}.$$

Here $\dot{N}_{\text{burn}} = P_{\text{fus}}/(E_{\text{DT}}\, f_b)$ is fixed by the fusion power and the fractional burn-up f_b; at $P_{\text{fus}} = 85.04\,MW$ the frozen burn rate is $\dot{N}_{\text{burn}} = 4.769\,kg\,\text{T}\,\text{fpy}^{-1}$ (BR-L1-A6). The breeding source is $\dot{N}_{\text{bred}} = \text{TBR}\cdot\dot{N}_n$ with $\dot{N}_n$ the $14\,MeV$ neutron rate and TBR the net blanket tritium-breeding ratio. The loss term $\dot{N}_{\text{loss}}$ is the sum of processing losses and the in-vessel permeation flux integrated over the first-wall area — the quantity this paper computes.

Writing the fractional loss $\varepsilon \equiv \dot{N}_{\text{loss}}/\dot{N}_{\text{bred}}$, the steady-state ($\mathrm{d}I_T/\mathrm{d}t = 0$, decay folded into ε at leading order) surplus per unit time is

$$\dot{S} = \dot{N}_{\text{burn}}\left[\text{TBR}\,(1-\varepsilon) - 1\right] = \dot{N}_{\text{burn}}\,\Lambda, \qquad \boxed{\Lambda \equiv \text{TBR}\,(1-\varepsilon) - 1 \;\geq\; 0}$$

which is the *self-sufficiency condition* on the net TBR with losses ε: the plant closes its own fuel cycle when $\Lambda \geq 0$, and exports a surplus $\dot{S} = \dot{N}_{\text{burn}}\Lambda$ otherwise. Equation (2) is the top-level ledger the accountancy twin must satisfy; the whole of the transport analysis below exists to supply ε (through the permeation loss) and to bound the in-vessel holdup that $\dot{N}_{\text{loss}}$ and I_T contain. The critical break-even ratio is $\text{TBR}_c = 1/(1-\varepsilon)$, so a per-cent-level loss shifts the self-sufficiency threshold by the same per cent.

IN-WALL TRANSPORT: MCNABB–FOSTER DIFFUSION–TRAPPING

The loss and holdup terms are set by hydrogen-isotope transport through the plasma-facing stack. Let $c_m(x,t)$ be the mobile (lattice-dissolved) tritium concentration and $c_{t,i}(x,t)$ the concentration trapped in trap population i. Conservation of mobile tritium with an implantation source $\Gamma(x,t)$ and trapping/detrapping exchange is the McNabb–Foster system [7]

$$\frac{\partial c_m}{\partial t} = \nabla\cdot\big(D(T)\,\nabla c_m\big) + \Gamma(x,t) - \sum_i \frac{\partial c_{t,i}}{\partial t},$$

$$\frac{\partial c_{t,i}}{\partial t} = \underbrace{\nu_0\, e^{-E_{d,i}/k_B T}}_{\text{trap rate } k_i} c_m\,\big(n_i - c_{t,i}\big) - \underbrace{\nu_0\, e^{-E_{p,i}/k_B T}}_{\text{detrap rate } p_i} c_{t,i},$$

where $D(T) = D_0\, e^{-E_D/k_B T}$ is the Arrhenius lattice diffusivity, n_i the density of trap i with detrapping energy $E_{p,i}$, and ν_0 an attempt frequency. Equations (3)–(3) are solved on the two-layer domain $x \in [0, L_{\text{W}} + L_{\text{E}}]$ with tungsten ($L_{\text{W}} = 0.5\,mm$) facing the plasma on Eurofer97-class RAFM steel ($L_{\text{E}} = 2\,mm$). The implantation source is a narrow band at the near-surface implantation range; for tritium at first-wall energies the range is a few nanometres, so on the millimetre scale the source is effectively a surface flux ϕ.

INTERFACE CONTINUITY AND BOUNDARY CONDITIONS

Tungsten and steel have very different solubilities, so the mobile concentration is discontinuous at the interface while the chemical potential is continuous. In the Sieverts (dilute) regime the partial pressure $p = (c_m/S)^2$ with solubility $S(T) = S_0\, e^{-E_S/k_B T}$, and continuity of chemical potential across the W/Eurofer interface $x = L_{\text{W}}$ reduces to continuity of the Sieverts partial pressure,

$$\left(\frac{c_m^{\text{W}}}{S_{\text{W}}(T)}\right)^2 = \left(\frac{c_m^{\text{E}}}{S_{\text{E}}(T)}\right)^2 \quad\Longrightarrow\quad \frac{c_m^{\text{W}}}{c_m^{\text{E}}} = \frac{S_{\text{W}}(T)}{S_{\text{E}}(T)},$$

implemented in FESTIM as a conservative chemical-potential (`chemical_pot`) interface. The plasma-side surface ($x = 0$) carries the implantation source and recombinative re-emission; the coolant-side surface ($x = L_{\text{W}} + L_{\text{E}}$) is held at low concentration (fast recombination), which is the conservative bound for the permeation flux and is the boundary against which breakthrough is defined.

STEADY PERMEATION: THE TWO-LAYER SERIES-RESISTANCE LIMIT

At steady state the tritium flux J is uniform through the stack. For each layer j the permeability is $\mathcal{P}_j(T) = D_j(T)\,S_j(T)$ and its permeation resistance is $R_j = L_j/\mathcal{P}_j$. In the diffusion-limited implantation regime the layers act as series resistances driven by the implantation source, and the steady permeation flux is

$$J = \frac{\phi\,R_\mathrm{p}}{L_\mathrm{W}}, \qquad R_\mathrm{p} = \frac{R_\mathrm{W}}{R_\mathrm{W}+R_\mathrm{E}} = \frac{L_\mathrm{W}/\mathcal{P}_\mathrm{W}}{L_\mathrm{W}/\mathcal{P}_\mathrm{W}+L_\mathrm{E}/\mathcal{P}_\mathrm{E}},$$

where R_p is the fraction of the implanted flux that permeates rather than re-emits. Because tungsten has a far larger E_D+E_S and lower permeability than Eurofer97 over 600–$800\,K$, the solubility partition is $S_\mathrm{W}/S_\mathrm{E} \sim 10^{-4}$–$10^{-5}$ and $R_\mathrm{W} \gg R_\mathrm{E}$, so $R_\mathrm{p} \to 1$ from below and the stack is *tungsten-diffusion-limited*: the Eurofer layer adds negligible resistance. Equation (5) makes the two operational facts explicit: the steady permeation flux is *temperature-independent* (the Arrhenius factors of D and S cancel in the diffusion-limited fraction to leading order) and *exactly linear in the wall load* ϕ. The finite-element solution is verified against (5) below.

BREAKTHROUGH (LAG) TIME

The transient before the steady flux is established is set by the diffusion time across the rate-limiting tungsten layer. The classical diffusion (time-lag) result gives a breakthrough time

$$\tau_\mathrm{bt} \simeq \frac{L_\mathrm{W}^2}{6\,D_\mathrm{W}(T)} = \frac{L_\mathrm{W}^2}{6\,D_{0,\mathrm{W}}}\,e^{E_{D,\mathrm{W}}/k_BT},$$

so the in-vessel inventory settles to quasi-steady within a diffusion time of a burn start. With $L_\mathrm{W} = 0.5\,mm$ and the tungsten diffusivity of Table 1, (6) predicts $\tau_\mathrm{bt} \approx 192\,s$ at $600\,K$ and $29\,s$ at $800\,K$ — the fast-settling behaviour that makes the tracked state well-posed rather than a slowly drifting unknown.

THE ACCOUNTANCY PROBLEM AS STATE ESTIMATION

Given the transport model, accountancy is a filtering problem. Collect the accountancy state $x = (I_T,\, I_\mathrm{wall},\, I_\mathrm{blkt},\, I_\mathrm{proc})^\top$ — plant mobile inventory, retained wall inventory, blanket-resident bred tritium, and processing-line inventory — evolving under the balance (1) driven by the computed transport fluxes,

$$\dot{x} = f(x, u, T), \qquad y_k = H x_k + \eta_k,$$

with actuator/operating inputs u (fuelling, temperature, pumping), plant diagnostics y_k (assays, flow meters, ionisation chambers, calorimetry) observed through H with noise η_k. The two transport terms that are not directly measured — I_wall and the permeation component of $\dot{N}_\mathrm{loss}$ — enter f through the FESTIM-computed budget of §4. The estimator is a Kalman/observer recursion on (7); in the linear-Gaussian limit the analysis update is

$$K_k = P_k^- H^\top (H P_k^- H^\top + R)^{-1}, \qquad \hat{x}_k^+ = \hat{x}_k^- + K_k(y_k - H\hat{x}_k^-), \qquad P_k^+ = (I - K_k H) P_k^-,$$

with R the diagnostic-noise covariance and P_k the state covariance [22]. The accountancy *closure* is the requirement that the innovation $y_k - H\hat{x}_k^-$ stay within safeguards tolerance; because I_wall and the permeation loss are supplied by known physics rather than fitted, the filter tracks a determined state rather than an open unknown.

§ 3

Computational methodology: the GPU-HPC campaign

FINITE-ELEMENT FORMULATION

Equations (3)–(4) are discretised and solved with FESTIM, an open-source finite-element hydrogen-transport code built on the FEniCS platform [12,13,14] (serial BR-L2-A25). Multiplying (3) by a test function $w \in H^1(\Omega)$ and integrating by parts gives the weak form: find $c_m \in H^1(\Omega)$ such that for all w,

$$\int_\Omega \frac{\partial c_m}{\partial t}\, w\,\mathrm{d}x + \int_\Omega D(T)\,\nabla c_m \cdot \nabla w\,\mathrm{d}x + \sum_i \int_\Omega \frac{\partial c_{t,i}}{\partial t}\, w\,\mathrm{d}x = \int_\Omega \Gamma\, w\,\mathrm{d}x + \int_{\partial\Omega_N} D(T)\,(\nabla c_m \cdot \quad n)\, w\,\mathrm{d}s,$$

with the trapped fields advanced by the pointwise ODEs (3). The domain is meshed with continuous Lagrange (P_1) elements on 573 nodes graded toward the plasma surface and the W/Eurofer interface, where the concentration gradients are steepest. The Sieverts interface (4) is imposed conservatively through the chemical-potential formulation, which carries the discontinuous mobile concentration without loss of flux continuity. Time integration uses backward Euler with adaptive steps; the nonlinear trapping coupling is resolved by a Newton iteration each step. The quantity of interest here — the steady permeation flux and the steady retained inventory — is obtained from the steady-state solve, which converged in $\sim 25\,s$ of wall time; the fully transient solve to physical steady state was consistent but stiff (adaptive stepping stalled near $t \sim 9 \times 10^4$ s), so the steady solver is used for the reported budget and the transient time-lag is taken from the analytic result (6).

MATERIAL PROPERTIES

The transport coefficients (Table 1) are literature values assembled through the `h-transport-materials` database. Tungsten uses Frauenfelder diffusivity and solubility [6] (the solubility extrapolated below its $1100\,K$ fit range, standard practice) with Ogorodnikova-class intrinsic traps [8]; Eurofer97 uses the Montupet-Leblond permeation/trapping data [11], whose 473–$673\,K$ fit range spans the wall temperature. No neutron-damage traps are included, which makes the retained inventory a lower bound (§8).

LAYER (SOURCE)	D_0 (M^2 S^{-1})	E_D (EV)	S_0 (M^{-3}PA$^{-1/2}$)	E_S (EV)	TRAPS (E_p; DENSITY)
W armour, $0.5\,mm$ [6,8]	4.1×10^{-7}	0.390	8.88×10^{23}	1.041	0.87 eV @ 1.3×10^{-3}; 1.00 eV @ 4×10^{-4}
Eurofer97, $2\,mm$ [11]	2.52×10^{-7}	0.160	1.06×10^{23}	0.27	0.80 eV @ 1×10^{-4}

Hydrogen-transport properties of the first-wall stack used in the FESTIM solve (BR-L2-A25). $\mathcal{P} = D_0 S_0\, e^{-(E_D+E_S)/k_B T}$ is the permeability; the large tungsten $E_D + E_S$ makes it the rate-limiting layer.

VERIFICATION AGAINST THE ANALYTIC LIMIT

FESTIM is verified against the exact steady two-layer series-resistance solution (5). Across all isothermal cases the code-to-analytic flux ratio is 1.000000 to seven significant figures, i.e. the finite-element steady flux reproduces the analytic diffusion-limited limit exactly within the model; the two-layer resistance ratio evaluates to $R_\mathrm{p} = 1.000000$ (Eurofer negligible). A dedicated TMAP8 code-to-code cross-check [15] was scoped but the local MOOSE/PETSc build was incomplete, so the independent verification is the analytic solution that the TMAP verification-and-validation suite itself uses as its reference; this is recorded as an open cross-code item rather than claimed as a completed second-code run. The independent analytic reproduction is what licenses the permeation loss as *exact within the model*.

THE NVIDIA GPU HPC CAMPAIGN

The frozen result set was produced under the Kronos NVIDIA GPU HPC campaign (Lambda fleet, A100/H100/A10), the same campaign that ran the surrounding neutronics, activation and materials gates so that all fuel-cycle numbers share one provenance chain. The tritium-transport gate (BR-L2-A25) ran the FESTIM/FEniCS solves — the nominal operating gradient, the isothermal $600/700/800\,K$ cases, and the wall-load sweep $\phi = 10^{20} \rightarrow 10^{21}\ \mathrm{T\,m^{-2}\,s^{-1}}$ — as a parameter batch, with the analytic verification evaluated alongside each solve. The upstream terms of the balance (1) are supplied by codes run on the same fleet: the $14\,MeV$ source and net TBR by OpenMC with DAGMC CAD geometry on ENDF/B-VIII.0 data [23,24], and the breeder-zone activation inventory — which underlies the bred-product separation of §6 — by the ALARA/PyNE/pypact activation chain (BR-L2-A23). GPU acceleration is used for the Monte-Carlo neutron transport (history-parallel) and for the parameter-batch orchestration; the finite-element transport solves themselves are modest and complete in seconds per case, so the campaign's value is throughput and one-provenance reproducibility rather than a single large solve. Every gate is archived with its run path and verdict in the register's reproducibility ledger, and no compute-cost information is part of this record.

§ 4

Results: the measured in-vessel tritium budget

THE BUDGET IN ONE TABLE

The FESTIM solve delivers the permeation loss and the retained inventory together (Table 2). These are the two transport quantities the balance (1) and the estimator (7)–(8) require, and they are computed rather than assumed. Figure 1 shows how they enter the plant balance.

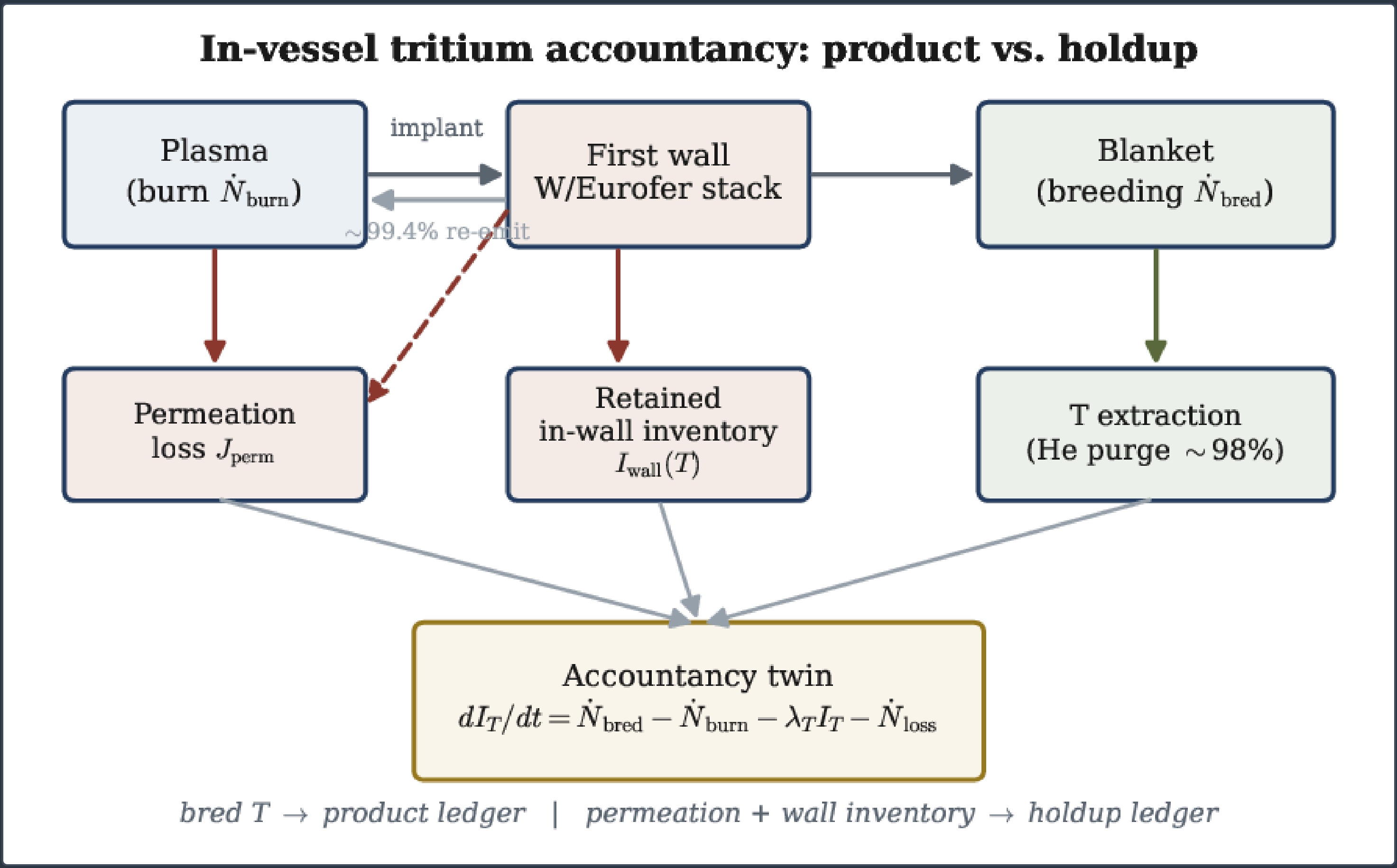

(Schematic.) The in-vessel tritium balance the accountancy twin closes. Bred tritium is credited to the *product* ledger; the permeation loss and the retained wall inventory are debited to the *holdup* ledger. Directed edges carry the terms of the balance equation (1); no data values are shown.

CASE	PERMEATION FLUX ($\mathrm{T\,m^{-2}\,s^{-1}}$)	RETAINED INVENTORY (T $\mathrm{M^{-2}}$)	BREAKTHROUGH
operating gradient (800 → 600 K)	5.16×10^{14}	1.75×10^{18} ($8.8\,\mu g/m^2$)	$\sim$30–190 s
isothermal 600 K (cold bound)	6.00×10^{14}	8.38×10^{19} ($0.42\,mg/m^2$)	$\sim$190 s
isothermal 700 K	6.00×10^{14}	6.2×10^{18}	—
isothermal 800 K	6.00×10^{14}	9.5×10^{17}	$\sim$30 s

FESTIM-computed in-vessel tritium budget for the $§I0.5

PERMEATION LOSS: DIFFUSION-LIMITED, TEMPERATURE-INDEPENDENT, LINEAR

The steady permeation flux is $5.16 \times 10^{14}\ \mathrm{T\,m^{-2}\,s^{-1}}$ in the nominal operating gradient case, equal to $0.082\,g\,\mathrm{T\,m^{-2}\,fpy^{-1}}$; only 0.52–0.60% of the implanted flux crosses the wall, with $\sim 99.4\%$ re-emitted to the plasma. Over a $\sim 100\,m^2$ first wall this is ~ 8–$10\,g\,\mathrm{T\,fpy^{-1}}$ passing into structure and coolant — a bounded holdup term for the fuel-cycle balance, small against the kilogram-scale surplus. The isothermal cases all give $6.00 \times 10^{14}\ \mathrm{T\,m^{-2}\,s^{-1}}$ (Figure 2): the diffusion-limited steady flux is temperature-independent, as equation (5) requires. Sweeping the wall load confirms exact linearity, $\phi = 10^{21}\ \mathrm{T\,m^{-2}\,s^{-1}} \Rightarrow J = 6.00 \times 10^{15}\ \mathrm{T\,m^{-2}\,s^{-1}}$ (Figure 2). The stack is tungsten-diffusion- limited: the tungsten permeation resistance exceeds Eurofer's by $\sim 3 \times 10^5$ over the operating window (Figure 3), so the two-layer series-resistance ratio is 1.000000 and the loss term is exact to the analytic limit.

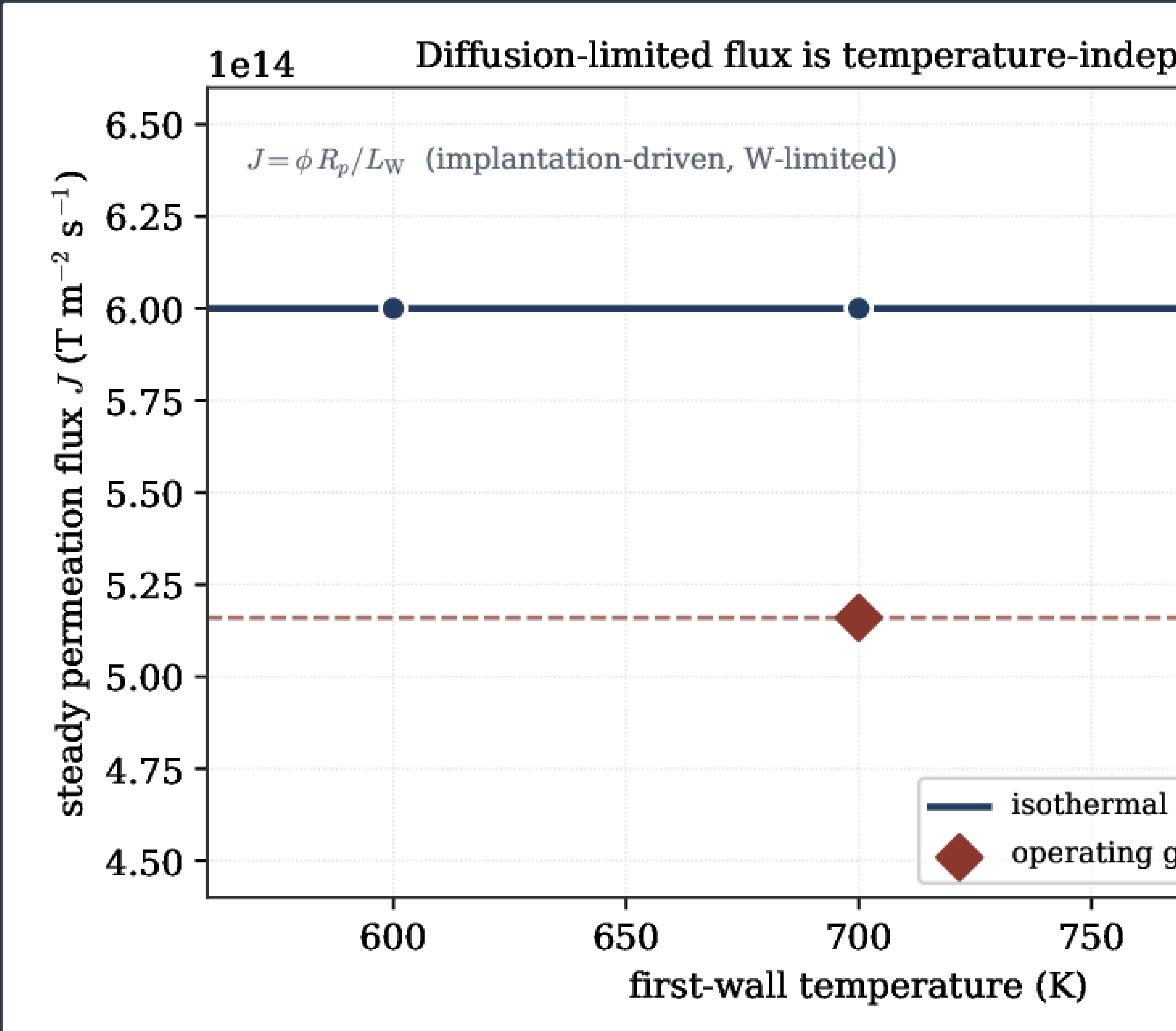
Diffusion-limited flux is temperature-indepe
1e14
$J = \phi R_p / L_W$ (implantation-driven, W-limited)
steady permeation flux J (T m^{-2} s^{-1})
6.50
6.25
6.00
5.75
5.50
5.25
5.00
4.75
4.50
600
650
700
750
first-wall temperature (K)
isothermal s
operating g

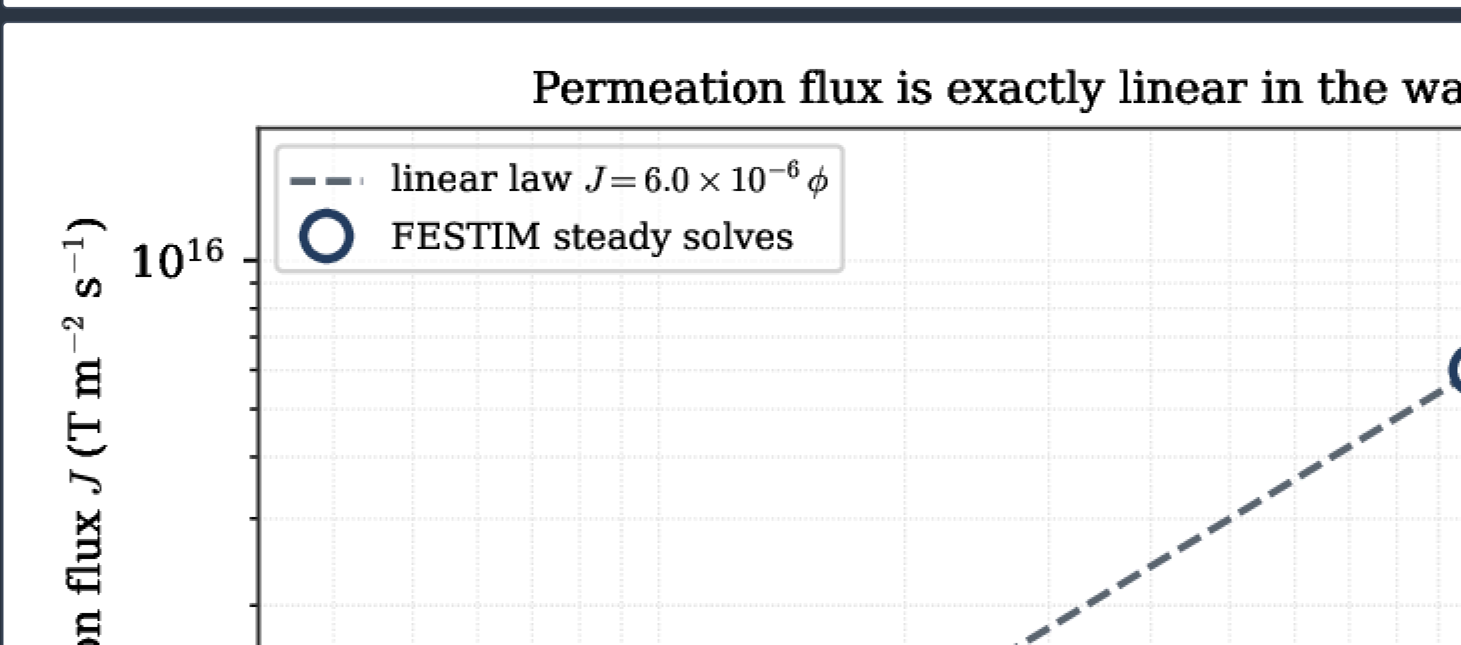
Permeation flux is exactly linear in the wal
linear law $J = 6.0 \times 10^{-6}\,\phi$
FESTIM steady solves
10^{16}
on flux J (T m^{-2} s^{-1})

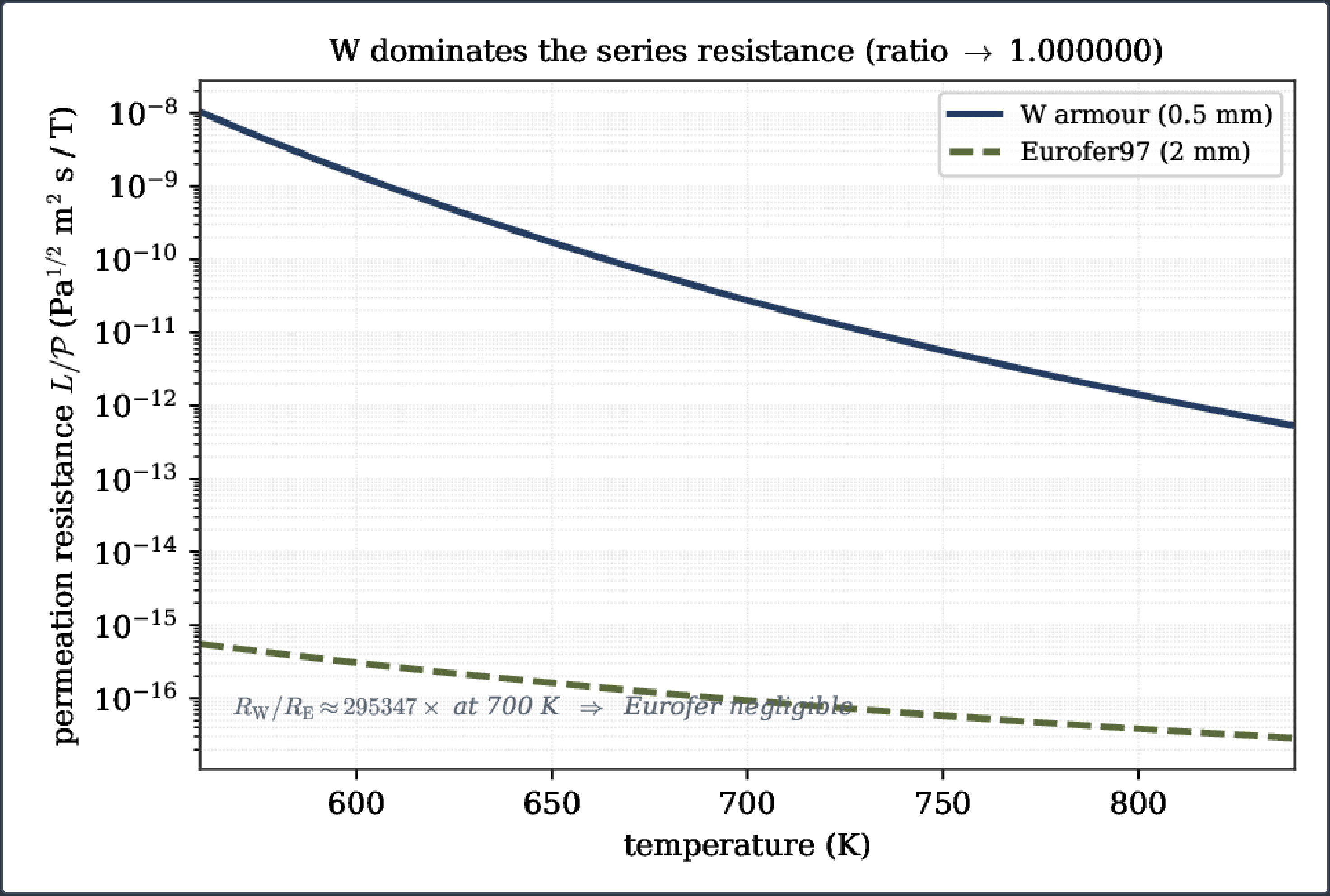

Series permeation resistance $L/\mathcal{P}$ of the tungsten armour and the Eurofer97 layer versus temperature, from the properties of Table 1. Tungsten dominates by $\sim 3 \times 10^5$ over 600–800 K, so the Eurofer layer is a negligible resistance and the stack is tungsten-diffusion- limited, giving the two-layer resistance ratio $R_\mathrm{p} = 1.000000$.

RETAINED INVENTORY: STRONGLY TEMPERATURE-DEPENDENT

The retained in-wall inventory is the quantity the estimator must follow, and it is a strong function of wall temperature (Figure 4). On the operating gradient the wall holds only $\approx 8.8\,\mu g/m^2$; in the cold $600\,K$ isothermal bound the tungsten traps fill and the inventory rises nearly two orders of magnitude to $0.42\,mg/m^2$; at $800\,K$ it falls to $9.5 \times 10^{17}\ \mathrm{T\,m^{-2}}$ ($\approx 4.8\,\mu g/m^2$). The high-energy tungsten trap (detrapping energy $1.0\,eV$) dominates the retained inventory, so a cold spot holds disproportionately more tritium than a hot one. Two operational conclusions follow directly: hot-wall operation *minimises* the held inventory, and the estimator must be *temperature-aware*, because the inventory hides where the wall runs cold.

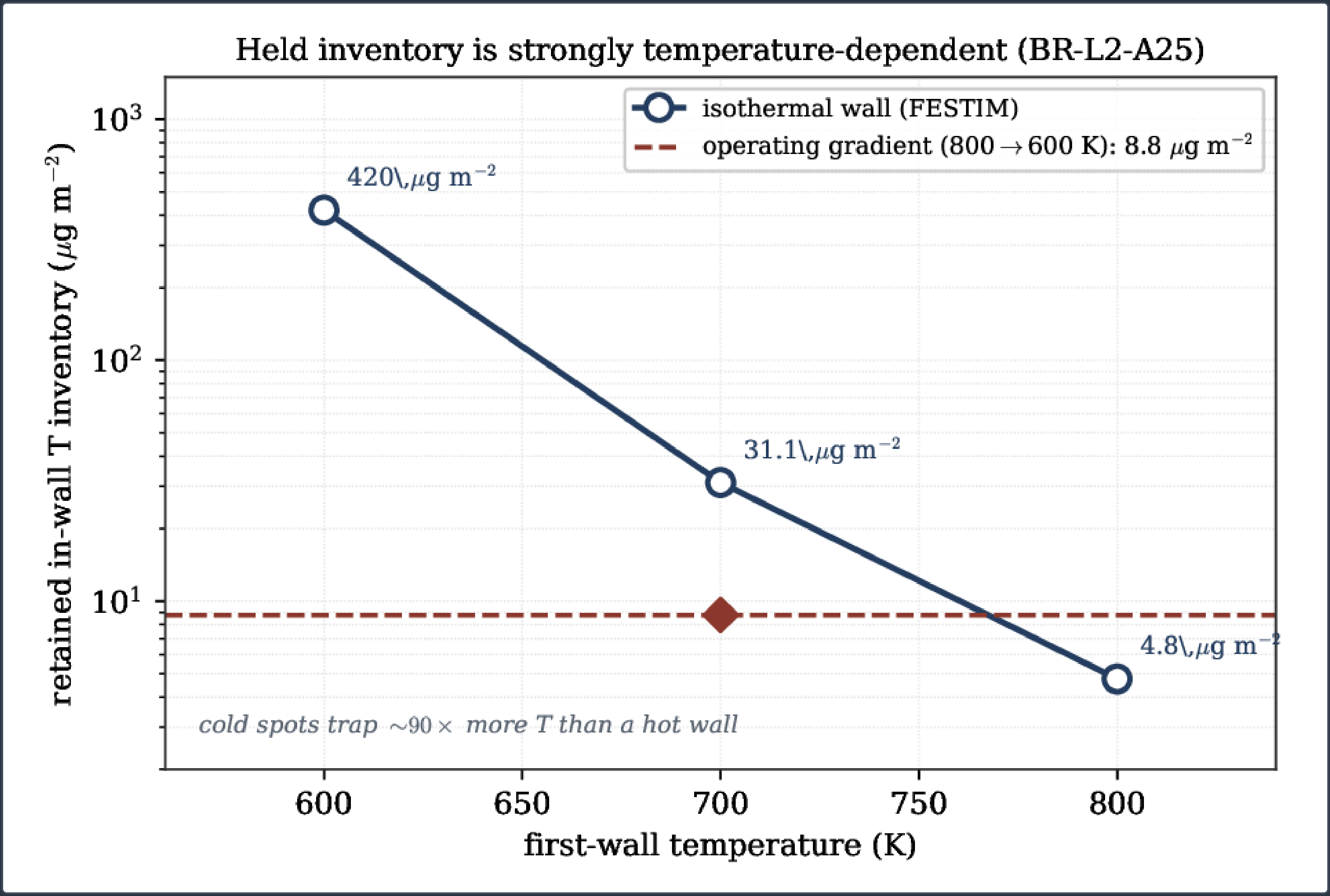

Retained in-wall tritium inventory versus first-wall temperature from the FESTIM solve (BR-L2-A25). Isothermal cases (markers) span nearly two orders of magnitude across $600–800\,K$; the operating- gradient case (dashed) sits near the hot end at $8.8\,\mu g/m^2$. Hot-wall operation minimises the held inventory.

BREAKTHROUGH: A FAST, WELL-POSED STATE

Breakthrough is fast — $\sim 190\,s$ at $600\,K$, $\sim 30\,s$ at $800\,K$ (Figure 5) — so the in-vessel inventory reaches quasi-steady within minutes of a burn start. The analytic time-lag law (6), evaluated with the tungsten diffusivity of Table 1, reproduces both frozen points ($192\,s$ and $29\,s$), confirming that the transient is governed by tungsten lattice diffusion. The twin therefore tracks a fast-settling state rather than a slowly drifting unknown — a property that matters for a safeguards estimator, which must be able to bound the inventory promptly after any operating-point change.

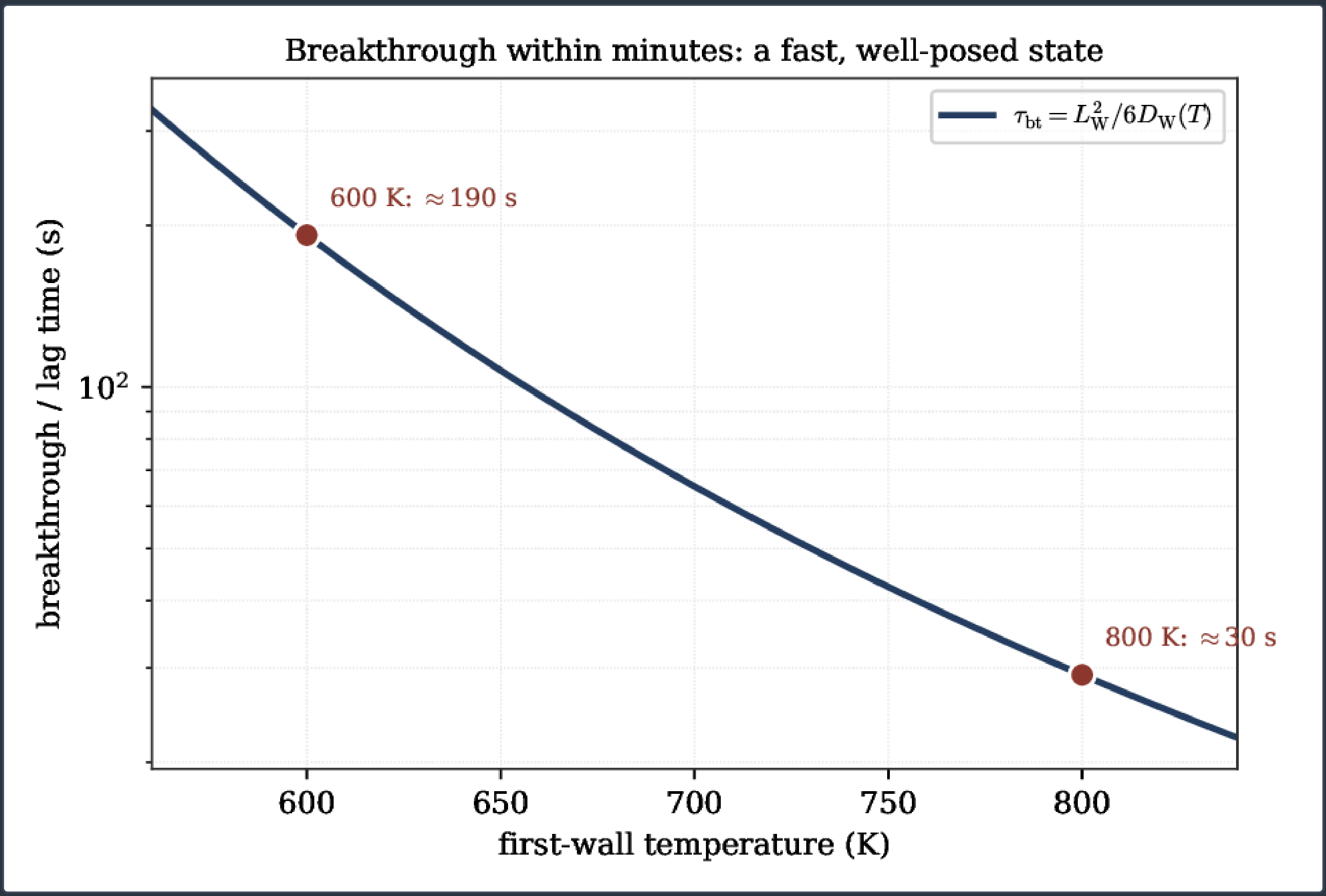

Breakthrough (time-lag) time versus wall temperature from equation (6) with the tungsten diffusivity of Table 1. Markers are the frozen FESTIM check points ($\sim 190\,s$ at $600\,K$, $\sim 30\,s$ at $800\,K$); the analytic curve reproduces both, so the inventory settles within minutes.

CLOSING THE TOP-LEVEL LEDGER: SURPLUS, SELF-SUFFICIENCY, AND START-UP

With the loss term fixed, the self-sufficiency condition (2) can be evaluated against the frozen breeding anchors (Figure 6). At $\dot{N}_{\mathrm{burn}} = 4.769\,kg\,\mathrm{T\,fpy}^{-1}$ the plant exports a surplus of $1.62\,kg\,\mathrm{T\,fpy}^{-1}$ at net $\mathrm{TBR} = 1.34$ and $3.82\,kg\,\mathrm{T\,fpy}^{-1}$ at $\mathrm{TBR} = 1.80$ (BR-L1-A6, BR-OUT-1); the per-cent-level permeation loss shifts the break-even ratio only to $\mathrm{TBR}_c \approx 1.002$. The honest-gate lower bound is also marked: an as-drawn net $\mathrm{TBR} = 0.742$ makes the plant a net tritium *consumer* that depletes a $2\,kg$ inventory in $1.49\,yr$ (BR-L1-A8), which is exactly the NO-GO the breeding-lever study resolves by adding a dedicated multiplier layer to reach net $\mathrm{TBR} \geq 1.05$ [doi:10.5281/zenodo.22645706]. The start-up inventory scales with the required reserve horizon (Figure 6): $2.38/4.77/9.54\,kg$ for reserve times of $0.5/1/2\,yr$ (BR-L1-A6), with the tritium-plant start-up itself at $\approx 1.07\,kg$ and an in-process inventory of $\approx 675\,g$ (BR-SX-17). These are the numbers the balance (1) integrates, and they are what the accountancy twin reconciles against the measured plant state.

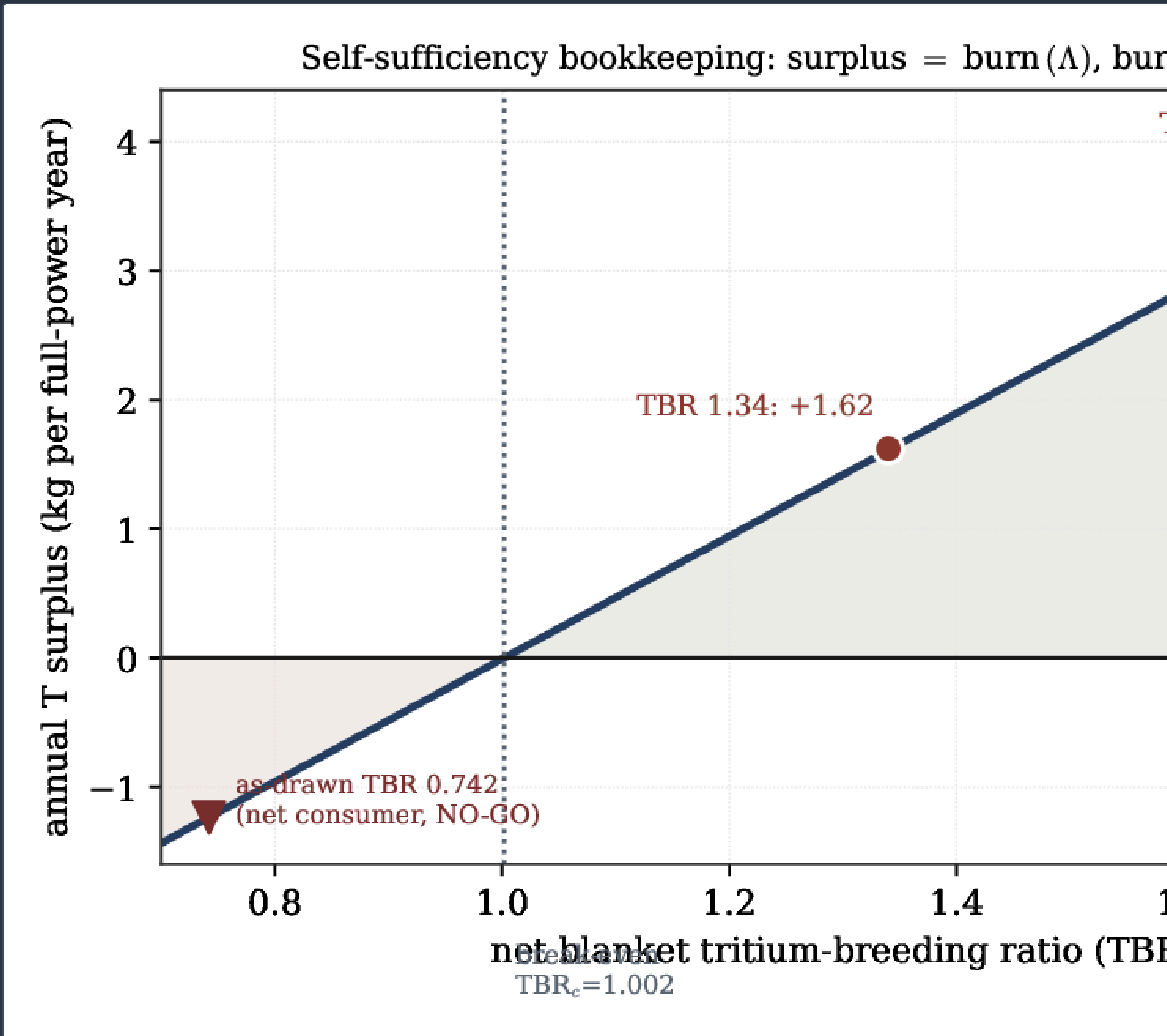
Self-sufficiency bookkeeping: surplus = burn (Λ), burn
annual T surplus (kg per full-power year)
4
3
2
1
0
−1
TBR 1.34: +1.62
as-drawn TBR 0.742
(net consumer, NO-GO)
0.8
1.0
1.2
1.4
net blanket tritium-breeding ratio (TBR
break-even
TBR$_c$=1.002

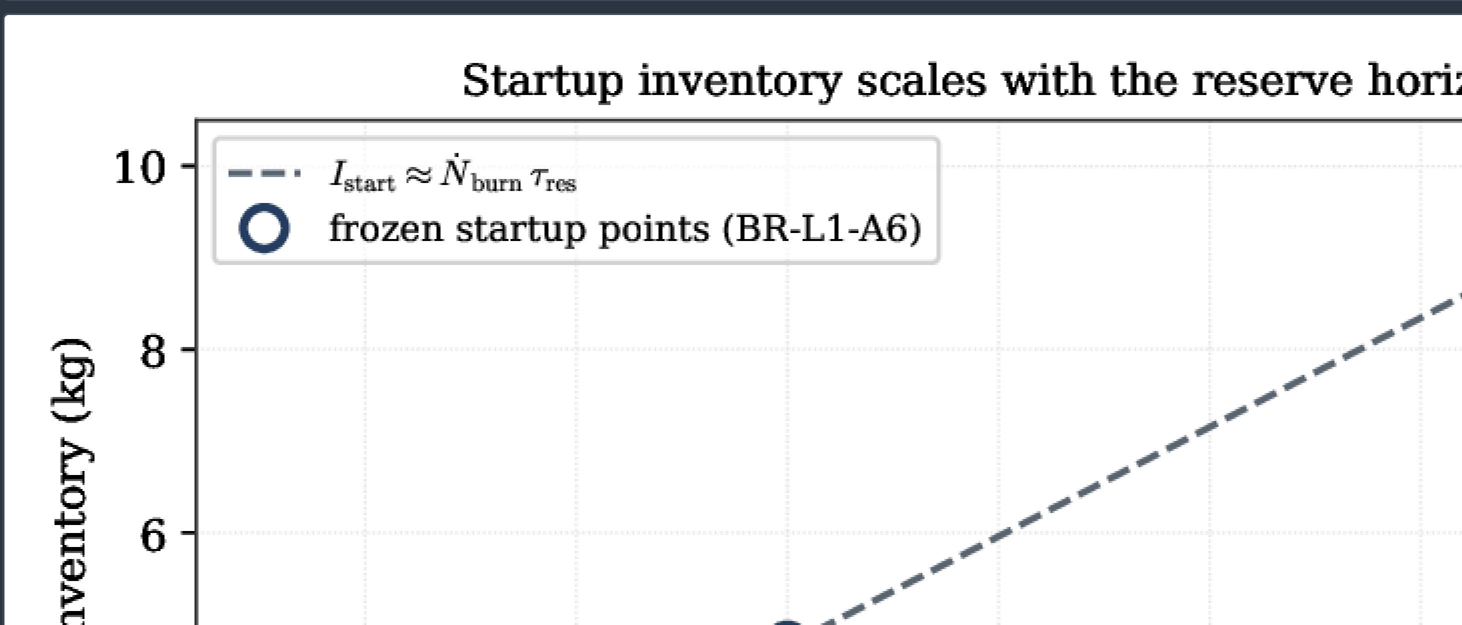
Startup inventory scales with the reserve horiz
$I_{start} \approx \dot{N}_{burn}\,\tau_{res}$
frozen startup points (BR-L1-A6)
10
8
6
nventory (kg)

§ 5

The accountancy twin

MODULE SET

On the measured budget we specify a real-time in-vessel tritium twin (Table 3). Each module runs the transport and inventory physics live against plant diagnostics and is admitted to authority only after it closes its balance to safeguards tolerance in simulation — the maturity-gated pattern of the Kronos control architecture [doi:10.5281/zenodo.22645805], applied to accountancy. Three modules carry the core balance; two coupled monitors extend it to the corrosion-transported and waste-classification terms that share the same neutronics/activation provenance (BR-L2-A23).

MODULE	PHYSICS ANCHOR	TRACKS	ACCEPTANCE TEST
real-time accountancy (BR-034)	FESTIM permeation (BR-L2-A25)	full T balance I_T	balance closes to safeguards tolerance
in-vessel inventory estimator (BR-081)	FESTIM retained inventory	held wall inventory $I_{\text{wall}}(T)$	inventory within safeguards tolerance
lithium-6 tracker	blanket supply ledger	Li-6 enrichment / inventory	balance matches supply ledger
corrosion / ACP monitor (BR-084)	activation transport (BR-L2-A23)	activated-corrosion-product inventory	ACP inventory within band
waste-classification twin (BR-085)	activation R2S (BR-L2-A23)	component waste class	class matches OpenMC/R2S in sim

The in-vessel tritium accountancy twin. Each module is anchored to a computed result and gated by an explicit closure test; serials refer to the register [31] and its Phase-1 control workplan.

COUPLING AND THE CLOSURE CONTRACT

The modules are coupled through the balance (1): the accountancy module's closure depends on the inventory estimator's held-inventory number $I_{\text{wall}}(T)$ and on the permeation loss, while the lithium-6 tracker anchors the breeding side of the ledger so that the tritium produced can be reconciled against the tritium accounted for. The corrosion and waste-classification monitors do not enter the tritium balance directly but share its neutronics/activation provenance, so admitting them on the same gate keeps one consistent activation state behind both the safeguards and the waste ledgers. The acceptance contract is a set of pre-registered inequalities, collected in Table 4: each module clears a closure test before it is granted authority, and control authority is capped by verification maturity until the test is met (Figure 7). Because the mapping from criterion to authority is explicit, the path from a verified estimator to a live safeguards instrument is a defined, testable sequence rather than an assertion.

CRITERION	BAR	ANCHOR	STATUS
permeation loss	exact to analytic two-layer limit	BR-L2-A25	**demonstrated** ($R_{\text{p}} = 1.000000$)
retained inventory	resolved function of T	BR-L2-A25	**demonstrated** (8.8 μg–0.42 mg m^{-2})
balance closure	innovation $\leq$ safeguards tolerance	BR-034	target
inventory closure	$\lvert\hat{I}_{\text{wall}} - I_{\text{wall}}\rvert \leq$ tolerance	BR-081	target
Li-6 tracking	matches blanket supply ledger	supply ledger	target
ACP monitor	inventory within band	BR-084	target
waste class	matches OpenMC/R2S in sim	BR-085	target

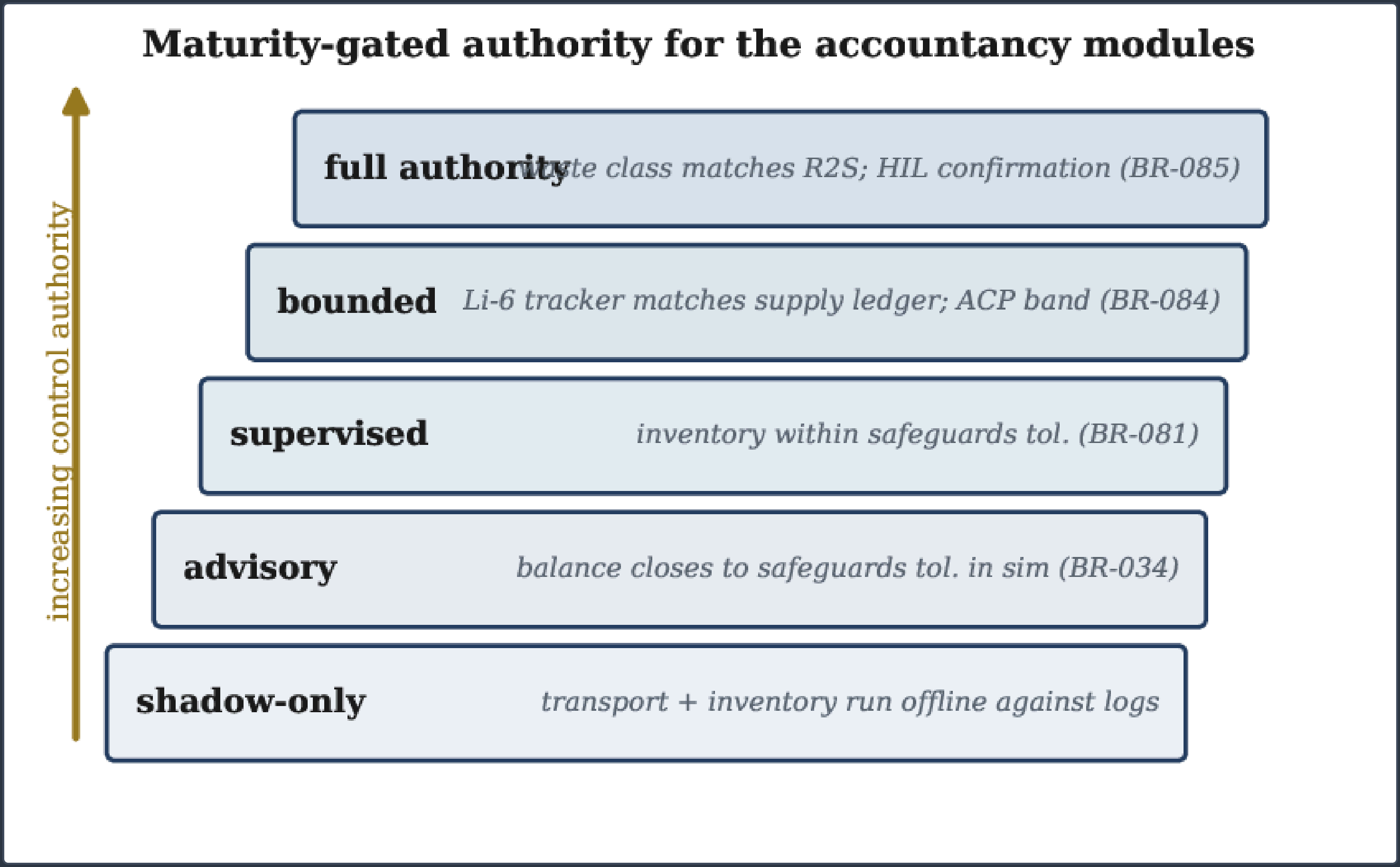

(Schematic.) Verification-maturity gating for the accountancy modules. Each rung admits a higher level of authority and is unlocked by the pre-registered closure tests of Table 4 (serials annotated). The closure bars are the real, frozen criteria; the authority ladder is a schematic of the gating policy.

§ 6

Separating product from holdup

Accountancy must not confuse tritium bred as *product* with tritium held as *holdup*. The breeder-zone activation inventory (BR-L2-A23) makes the distinction concrete: at long cooling times the breeder ceramic's residual activity is essentially all bred tritium held in the lithium ceramic — an artefact of no-purge bookkeeping, since in operation that tritium is the recovered product (He-purge extraction recovers $\sim$98% at a $\sim$10.9 *hour* pebble residence, giving an in-process ceramic inventory of $\sim$4.8 *g*; BR-CX-17), not waste. The accountancy twin encodes exactly this separation: bred tritium in the blanket is credited to the product ledger and routed to recovery, while the small permeation term and the trapped wall inventory are debited to the holdup ledger.

The scale separation is what makes the two ledgers reconcilable (Figure 8). The product terms are kilogram-scale — a breeding surplus of 1.62–$3.82\,kg\,\mathrm{T\,fpy}^{-1}$, a start-up inventory of order $1\,kg$, an in-process inventory of $\sim 675\,g$. The in-vessel holdup terms are grams and below — a permeation loss of 8–$10\,g\,\mathrm{T\,fpy}^{-1}$, and a retained wall inventory over the whole $100\,m^2$ first wall of only $\sim 0.9\,mg$ on the operating gradient (rising to $\sim 42\,mg$ in the cold bound). Keeping the two ledgers distinct is what lets the balance close simultaneously against the fuel cycle (which needs the surplus) and the safeguards frame (which needs the holdup bounded); the permeation-barrier wall-chemistry choice that holds the holdup ledger where Figure 8 places it is treated separately [doi:10.5281/zenodo.22645870].

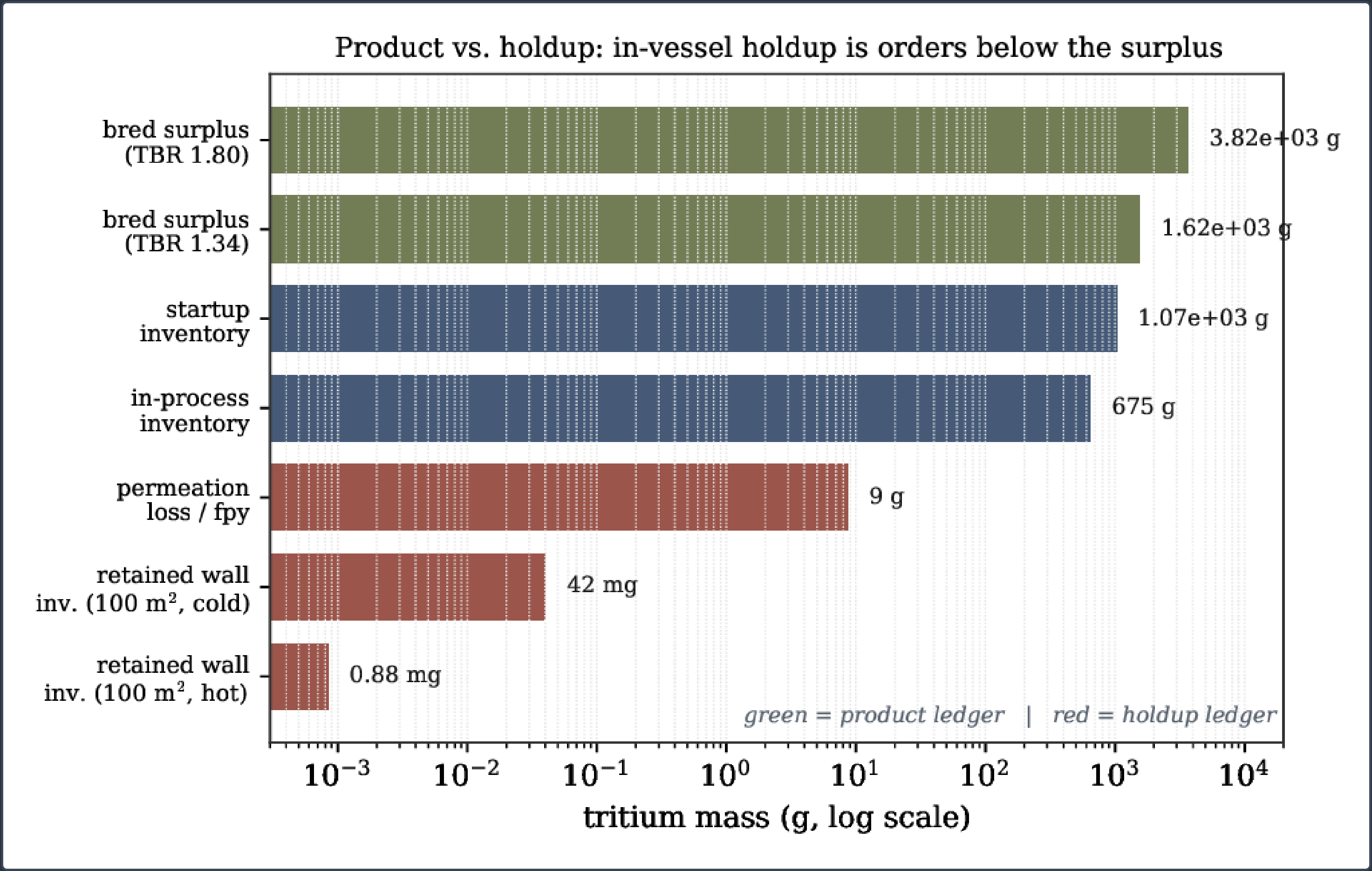

Product versus holdup ledger (log scale). The bred surplus, start-up and in-process inventories (product, green) are kilogram-scale; the permeation loss and the retained wall inventory (holdup, red) are grams and below. The orders-of-magnitude separation is what makes the two ledgers independently closable. Values from BR-L1-A6, BR-SX-17 and BR-L2-A25.

§ 7

Discussion

AGAINST THE PUBLISHED TRANSPORT AND SELF-SUFFICIENCY LITERATURE

The accountancy case is strong precisely because its two governing numbers are computed rather than fitted. The permeation loss is exact to the analytic two-layer limit and sits in a regime the transport literature would predict: with tungsten armour the stack is diffusion-limited, and the sub-per-cent permeation fraction ($0.52–0.60\%$) with $\sim 99.4\%$ re-emission is consistent with the strong recombination-limited re-emission seen for hydrogen on tungsten [9,10,8]. The retained inventory's temperature dependence — a near-two-order-of-magnitude rise from a hot to a cold wall, dominated by the $1.0\,eV$ tungsten trap — is the expected signature of high-energy intrinsic traps filling as detrapping slows, and identifies the operationally useful lever (run the wall hot). At the systems level, the self-sufficiency framing of equation (2) is the same $\Lambda = \mathrm{TBR}(1-\varepsilon) - 1$ condition analysed for DEMO-class plants [16,17]; our contribution is to supply ε from a first-principles in-vessel transport solve and to show that at $\sim 8–10\,g\,\mathrm{T}\,\mathrm{fpy}^{-1}$ the first-wall permeation term moves the break-even ratio by only $\sim 0.2\%$, so it is not the term that decides self-sufficiency — the net TBR is. This is consistent with the global tritium-supply picture, in which start-up inventory of order a kilogram, not steady in-vessel permeation, is the binding constraint [18,19].

WHAT THE TWIN ADDS

Relative to a periodic mass-balance audit, the twin turns accountancy into a continuously closed balance. Three properties make that feasible here and not in general. First, the tracked in-vessel state is *fast*: equation (6) and Figure 5 show breakthrough within minutes, so the estimator never has to extrapolate a slowly drifting hidden inventory. Second, it is *well-posed*: the loss term is exact and the inventory is a resolved function of a measured quantity (wall temperature), so the filter (8) assimilates diagnostics against known physics rather than fitting an open unknown. Third, it is *scale- separated*: Figure 8 shows the holdup ledger sits orders of magnitude below the product ledger, so a bounded, computed holdup term cannot corrupt the kilogram-scale surplus accounting. Together these let the twin report a calibrated inventory with a credible-interval bound, which is what a safeguards frame reads.

§ 8

Limitations

One honest gate bounds the retained-inventory claim: the FESTIM solve omits neutron-damage traps and is therefore a *lower bound* on the held inventory. Irradiation-induced traps in tungsten can raise the retained inventory by one-to-two orders of magnitude as displacement damage accumulates; the twin accommodates this by carrying a damage-dependent trap population that grows with fluence, so the inventory estimate is conservative until the damage-trap term is folded in. Crucially, the *steady permeation loss is unaffected* — traps delay the flux but do not change its steady value — so the loss term, and with it the self-sufficiency bookkeeping of equation (2), stands as computed while only the inventory estimate carries the damage-trap conservatism. The independent verification of the loss term is analytic rather than a second code: the TMAP8 cross-check is scoped but not completed, and is recorded as an open cross-code item.

§ 9

Conclusion

The in-vessel tritium budget of a compact spherical-tokamak breeder is a computed, well-posed, fast-settling state. A FESTIM finite-element solve of the actual $0.5\,mm\,\mathrm{W} + 2\,mm$ Eurofer first-wall stack fixes the permeation loss at $5.16 \times 10^{14}\,\mathrm{T\,m^{-2}\,s^{-1}}$ ($0.082\,g\,\mathrm{T\,m^{-2}\,fpy^{-1}}$, exact to the analytic two-layer limit, temperature-independent and linear in wall load) and the retained inventory at $8.8\,\mu\,g/m^2$ on the operating gradient — strongly temperature-dependent and lowest at a hot wall — with breakthrough within $30\text{–}190\,s$. Integrated over the first wall the permeation term is $\sim 8\text{–}10\,g\,\mathrm{T\,fpy^{-1}}$, orders below the $1.62\text{–}3.82\,kg\,\mathrm{T\,fpy^{-1}}$ breeding surplus, so it moves the self-sufficiency threshold by only $\sim 0.2\%$. On this measured budget the accountancy twin — a real-time balance, an in-vessel inventory estimator, a lithium-6 tracker, and coupled corrosion and waste-classification monitors, each gated to close to safeguards tolerance — closes the tritium books live, separating the tritium bred as product from the tritium held as holdup so that one balance satisfies both the fuel cycle and the safeguards frame.

Acknowledgments tocsectionAcknowledgments Part of the Kronos Fusion Energy 2026 design series. The author thanks the Kronos physics de-risking programme for the frozen result set underlying every quantitative claim, and the FESTIM and OpenMC communities for the open-source codes on which the transport and neutronics gates run.

Reproducibility. The permeation and inventory numbers are frozen results (BR-L2-A25, FESTIM/FEniCS) in the Kronos Physics De-Risking Register [31] (doi:10.5281/zenodo.22133057), regenerable from the archived FESTIM driver and verified against the analytic two-layer series-resistance solution; the bred-product separation draws on the breeder-zone activation inventory (BR-L2-A23), and the fuel-cycle anchors on BR-L1-A6, BR-OUT-1 and BR-SX-17. The accountancy modules are the tritium cluster of the Kronos AI/ML control architecture. The figure-generation script and its inputs are deposited with this paper. This paper is archived at its DOI doi:10.5281/zenodo.22645876; official version: https://www.kronosfusionenergy.com/publications/a-real-time-tritium-accountancy-twin-for-a-compact-sphe.html and its official page kronosfusionenergy.com/publications/a-real-time-tritium-accountancy-twin-for-a-compact-sphe.html; the de-risking register is DOI doi:10.5281/zenodo.22133057.

Data availability tocsectionData availability The FESTIM inputs, the computed budget, and the figure data are archived with the deposit at doi:10.5281/zenodo.22645876, which references the Kronos 2026 series register [31] (doi:10.5281/zenodo.22133057) and the AI/quantum-control deposit [32] (doi:10.5281/zenodo.21842371). Any economic analysis is reported separately and is not part of the public deposit.

Competing interests tocsectionCompeting interests Provisional patent applications relating to aspects of this work have been filed.

tocsectionReferences

APPARATUS

Portfolio, People & Record

The intellectual-property estate, the people who built it, the limitations that gate it, and the sources it rests on.

1	4	40	27
GRANTED PATENT	2026 PROVISIONALS	TEAM MEMBERS	2022 PROVISIONALS

INTELLECTUAL PROPERTY

The patent portfolio

The estate spans a granted high-field magnet patent, pending utility and 2026 provisional filings that map to the two products, a digital-twin control provisional, a registered trademark application, and the original 2022 provisional family. Every patentable disclosure in the five-paper arXiv drop was protected **before** publication: the breeder and burner provisionals were filed 1–2 August, and a publication-gap omnibus filing the evening before the drop swept up the DEC, plasma-control, and REBCO-winding matter of the three otherwise-unprotected papers. Patent numbers and application serials are matters of public record; claim scope is summarised, not reproduced.

GRANTED & PENDING UTILITY

US 12,009,112	High-field tilted graded-REBCO magnet architecture (KRONO-002A) · *app. 17/878,550*	GRANTED
US 17/878,507	Core device / method (KRONO-001A) · *utility*	PENDING

2026 PROVISIONAL FILINGS — MAPPED TO THE PRODUCTS

64/124,209	Hyperion — spherical-tokamak tritium / helium-3 foundry · *breeder · filed Aug 2026*	FILED
64/124,220	Aegis / MetroVolt — synchrotron-cutoff, fuel-selection & plug-winding · *generator · filed Aug 2026*	FILED
64/115,167	KRONOS-CTRL digital-twin plant control · *provisional · filed Jul 2026*	FILED
64/005,440	Integrated spherical-tokamak fusion architecture · *early integrated-architecture filing · filed Mar 2026*	FILED
64/105,530	Negative-triangularity spherical-tokamak architecture · *foundational ST filing · filed Jul 2026*	FILED
64/128,097	Publication-gap omnibus — quasineutral two-species expander DEC · provenance-gated / latency-split plasma control · as-built high-field winding & conductor architecture · *filed 7 Aug 2026, the evening before the arXiv drop*	FILED

TRADEMARK & ORIGIN

FTK-98801894	Kronos Fusion Energy — trademark application	FILED
KR-2022-*	Original provisional family (KR-2022-00001 … 00027) · *27 filings, 2022*	PRIORITY

The narrow, defensible magnet novelty — the specific conductor and the digital-twin winding optimisation, not high-field REBCO as a category — is the commercial core that can earn ahead of any Q > 1 milestone, with markets in fusion magnet supply, MRI/NMR, accelerators, and proton therapy. The claim is scoped honestly: the high field is a *system field* result, not a stand-alone-coil record; the small-bore plug coil is structurally infeasible as a bare winding but resolved by a stress-managed structural shield (feasible-pending-FEA); and the winding-tape experiment returned a *null result*. The value is the method, not a field record.

THE TEAM

Founding partners, board, advisors & auditors

Kronos is built by a bench of advanced-fuel-fusion, high-field-magnet, direct-conversion, and materials specialists, with a board and operations team drawn from defense, national laboratories, and industry. Dates are shown as ranges; where a tenure has ended or is term-ending, the range says so.

FOUNDING PARTNERS — SCIENCE

Dr. Gerald Kulcinski
Co-Founder · Helium-3 & Advanced-Fuel Fusion
UW–Madison · 2023–Present

Dr. Carl Weggel
Chief Scientist / S.M.A.R.T. Design
MIT Alcator Program · 2022–Present

Dr. Robert J. Weggel
Magnetic Field Design
MIT Magnet Lab · 2022–Present

BOARD

Priyanca Ford
Founder & CEO · Executive Board
2022–Present

Bandel Carano
Finance / Strategy
Oak Investment Partners / Stanford · 2025–2026

Patrick Schweiger
Fusion Device Engineering
Oklo / CFS / TerraPower · 2025–Present

SCIENTIFIC ADVISORS

Dr. Steven O. Dean
Fusion Policy & History
DOE / Fusion Power Associates · 2025–Present

Dr. Patrick H. Diamond
Plasma Turbulence & Transport
UC San Diego · 2025–Present

Dr. Jack J. Dongarra
HPC & Numerical Algorithms
Turing Award · 2025–Present

Dr. Nasr M. Ghoniem
Chief Material Scientist
UCLA · 2025–Present

Dr. Siegfried Glenzer
Plasma Physics & Laser Fusion
Stanford / SLAC · 2022–Present

Dr. David A. Hammer
Pulsed-Power Fusion
Cornell · 2025–Present

Dr. Donald A. Spong
Plasma Theory & Confinement
ORNL · 2025–Present

Dr. Curtis Smith
Risk Assessment & Nuclear PRA
MIT / Idaho National Lab · 2025–Present

RADM (Ret.) David Goggins
Naval Engineering & Power-Plant Design
U.S. Navy · 2023–2026

Dr. Konstantin Batygin
Mathematician
Caltech · 2022–2025

Dr. Ruben Fair
Magnet Design / ITER Liaison
PPPL / Jefferson Lab · 2022–2025

Dr. Paul S. Weiss
Materials & Nanotechnology
UCLA · 2022–2025

SCIENTIFIC AUDITORS

Dr. Wilfred A. Cooper
Plasma Equilibrium Theory
EPFL / Swiss Plasma Center · 2025–Present

Dr. Ahmed Hassanein
Plasma–Material Interactions
Purdue / Argonne · 2025–Present

Dr. Patrick E. Hopkins
Extreme Thermal Materials
U. of Virginia · 2025–Present

Dr. Peter Hosemann
Materials Joining & Structural Integrity
UC Berkeley · 2025–Present

Dr. Travis W. Knight
Advanced Nuclear Fuels & Systems
U. of South Carolina · 2025–Present

Dr. Philippe Lebrun
Cryogenics & Magnet Cooling
CERN · 2025–Present

Dr. Nitendra Singh
Nuclear Safety & Fuel Cycle
ITER · 2025–Present

Dr. Guido Van Oost
Magnetic Confinement & Fusion Systems
Ghent University · 2025–Present

Dr. Gary S. Was
Radiation Materials & Structural Integrity
U. of Michigan · 2025–Present

Dr. Ray Sedwick
Direct Energy Conversion
U. of Maryland · 2025

OPERATIONS

Michael Laughlin
Chief Operating Officer
2022–Present

Martin Owens
Chief Strategy Officer
LANL / GE Hitachi · 2022–Present

MG (Ret.) Paul Pardew
Chief Contracting Officer
Army Contracting Command · 2022–Present

David Beck
Fusion Commercialization
U.S. Space Force · 2024–Present

Sushma Bhatia
Environmental & Legislative
Google · 2022–Present

Michael De Frenza
Technology Licensing
2023–Present

MG (Ret.) Robin L. Fontes
Cybersecurity & Defense
Army Cyber Command · 2022–Present

Vijay Gehani
Supply Chain & Components
INOX India · 2024–Present

Jon Michel Greenwood
IT & AI Infrastructure
Live Nation · 2023–Present

Brian C. O'Neill
National Security
CIA / ODNI · 2022–Present

Gen. (Ret.) Gustave F. Perna
DoD Liaison
Operation Warp Speed · 2022–2023

Andrea Romero
Marketing Lead
2022–Present

Legal counsel is retained; those roles are held on the internal roster and are not listed here.

SOURCES

References

1 L L Lucas and M P Unterweger, Comprehensive review and critical evaluation of the half-life of tritium, *J. Res. Natl. Inst. Stand. Technol.* **105** 541 (2000). doi:10.6028/jres.105.043

2 J E Menard *et al*, Fusion nuclear science facilities and pilot plants based on the spherical tokamak, *Nucl. Fusion* **56** 106023 (2016). doi:10.1088/0029-5515/56/10/106023

3 B N Sorbom *et al*, ARC: a compact, high-field, fusion nuclear science facility and demonstration power plant with demountable magnets, *Fusion Eng. Des.* **100** 378 (2015). doi:10.1016/j.fusengdes.2015.07.008

4 M E Austin *et al*, Achievement of reactor-relevant performance in negative triangularity shape in the DIII-D tokamak, *Phys. Rev. Lett.* **122** 115001 (2019). doi:10.1103/PhysRevLett.122.115001

5 A Marinoni, O Sauter and S Coda, A brief history of negative triangularity tokamak plasmas, *Rev. Mod. Plasma Phys.* **5** 6 (2021). doi:10.1007/s41614-021-00054-0

6 R Frauenfelder, Solution and diffusion of hydrogen in tungsten, *J. Vac. Sci. Technol.* **6** 388 (1969). doi:10.1116/1.1492699

7 A McNabb and P K Foster, A new analysis of the diffusion of hydrogen in iron and ferritic steels, *Trans. Metall. Soc. AIME* **227** 618 (1963).

8 O V Ogorodnikova, J Roth and M Mayer, Deuterium retention in tungsten in dependence of the surface conditions, *J. Nucl. Mater.* **313–316** 469 (2003). doi:10.1016/S0022-3115(02)01375-2

9 R A Causey, Hydrogen isotope retention and recycling in fusion reactor plasma-facing components, *J. Nucl. Mater.* **300** 91 (2002).

10 J Roth and K Schmid, Hydrogen in tungsten as plasma-facing material, *Phys. Scr.* **T145** 014031 (2011).

11 F Montupet-Leblond *et al*, Permeation and trapping of hydrogen in Eurofer97, *Nucl. Mater. Energy* **29** 101062 (2021). doi:10.1016/j.nme.2021.101062

12 R Delaporte-Mathurin, E A Hodille, J Mougenot, Y Charles and C Grisolia, Finite element analysis of hydrogen retention in ITER plasma facing components using FESTIM, *Nucl. Mater. Energy* **21** 100709 (2019). doi:10.1016/j.nme.2019.100709

13 R Delaporte-Mathurin, J Dark, G Ferrero, E A Hodille, V Kulagin and S Meschini, FESTIM: an open-source code for hydrogen transport simulations, *Int. J. Hydrogen Energy* **63** 786 (2024). doi:10.1016/j.ijhydene.2024.03.184

14 M S Aln s *et al*, The FEniCS Project version 1.5, *Arch. Numer. Software* **3** 100 (2015). doi:10.11588/ans.2015.100.20553

15 G R Longhurst, *TMAP7 User Manual*, Idaho National Laboratory report INL/EXT-04-02352 (rev. 2008).

16 M Abdou *et al*, Physics and technology considerations for the deuterium–tritium fuel cycle and conditions for tritium fuel self-sufficiency, *Nucl. Fusion* **61** 013001 (2021). doi:10.1088/1741-4326/abbf35

17 M E Sawan and M A Abdou, Physics and technology conditions for attaining tritium self-sufficiency for the DT fuel cycle, *Fusion Eng. Des.* **81** 1131 (2006). doi:10.1016/j.fusengdes.2005.07.035

18 M Kovari, M Coleman, I Cristescu and R Smith, Tritium resources available for fusion reactors, *Nucl. Fusion* **58** 026010 (2018). doi:10.1088/1741-4326/aa9d25

19 R J Pearson, A B Antoniazzi and W J Nuttall, Tritium supply and use: a key issue for the development of nuclear fusion energy, *Fusion Eng. Des.* **136** 1140 (2018). doi:10.1016/j.fusengdes.2018.04.090

20 M Glugla *et al*, The ITER tritium systems, *Fusion Eng. Des.* **82** 472 (2007). doi:10.1016/j.fusengdes.2007.02.025

21 M G Kapteyn, J V R Pretorius and K E Willcox, A probabilistic graphical model foundation for enabling predictive digital twins at scale, *Nat. Comput. Sci.* **1** 337 (2021). doi:10.1038/s43588-021-00069-0

22 R E Kalman, A new approach to linear filtering and prediction problems, *J. Basic Eng.* **82** 35 (1960). doi:10.1115/1.3662552

23 P K Romano and B Forget, The OpenMC Monte Carlo particle transport code, *Ann. Nucl. Energy* **51** 274 (2013). doi:10.1016/j.anucene.2012.06.040

24 P K Romano, N E Horelik, B R Herman, A G Nelson, B Forget and K Smith, OpenMC: a state-of-the-art Monte Carlo code for research and development, *Ann. Nucl. Energy* **82** 90 (2015). doi:10.1016/j.anucene.2014.07.048

25 A Logg, K-A Mardal and G N Wells (eds), *Automated Solution of Differential Equations by the Finite Element Method*, Springer, Berlin (2012). doi:10.1007/978-3-642-23099-8

26 R A Causey, R A Karnesky and C San Marchi, Tritium barriers and tritium diffusion in fusion reactors, in *Comprehensive Nuclear Materials* vol. 4, Elsevier, p. 511 (2012). doi:10.1016/B978-0-08-056033-5.00116-6

27 C Day and T Giegerich, The direct internal recycling concept to simplify the fuel cycle of a fusion power plant, *Fusion Eng. Des.* **88** 616 (2013). doi:10.1016/j.fusengdes.2013.05.026

28 L L Lao, H St John, R D Stambaugh, A G Kellman and W Pfeiffer, Reconstruction of current profile parameters and plasma shapes in tokamaks, *Nucl. Fusion* **25** 1611 (1985). doi:10.1088/0029-5515/25/11/007

29 G Evensen, The ensemble Kalman filter: theoretical formulation and practical implementation, *Ocean Dyn.* **53** 343 (2003). doi:10.1007/s10236-003-0036-9

30 A J Creely *et al*, Overview of the SPARC tokamak, *J. Plasma Phys.* **86** 865860502 (2020). doi:10.1017/S0022377820001257

31 P I Ford, *Kronos Physics De-Risking Register*, Kronos Fusion Energy 2026 series. doi:10.5281/zenodo.22133057

32 P I Ford, *AI and quantum computing for fusion*, Kronos Fusion Energy 2026 design series. doi:10.5281/zenodo.21842371

COLOPHON

How this document was made

The Kronos Fleet — Combined Editorial, 2026 is set in **Fraunces** (display), **Gelasio** (text), and **IBM Plex Mono** (data & equations), carried forward from the Kronos editorial design system.

The figures are rendered at 300 dpi from the deposited generator scripts; the document is composed as a single self-contained file with embedded fonts and imagery, paginated to US Letter, and rendered to PDF through a headless Chromium engine in matched light and dark editions.

Every headline quantity carries an evidence class; withdrawn and restated values are marked as such. Nothing herein is frozen beyond the founder-approved Tier-A set.

Explore it live — turn the interactive 3-D model, run the deposited solvers in the physics validator, and watch the companion film series.

LEGAL NOTICE

Notice, status, and distribution

Conceptual design & simulation study. This document reports a conceptual design and simulation study. It is not a construction commitment, a safety-analysis report, a regulatory filing, or an offer of securities. Forward-looking statements — schedules, costs, market sizes, and performance — are estimates subject to the limitations set out in the Simulations part and may change.

Numbers and their classes. Quantities are reported with evidence classes and case labels; modelled, assumed, and requirement-class values are identified as such and are not to be quoted without their labels.

Public edition. This edition carries the physics and design only; all financial, funding, and defense-commercial content has been removed for public distribution. The scientific text corresponds to the arXiv and journal submissions.

THE 2026 KRONOS SERIES

One programme, many papers

This editorial is one paper in the Kronos 2026 series — a real fusion company's complete, reproducible physics record for a spherical-tokamak breeder and its low-neutron D–^{3}He tandem-mirror burners. Every headline number is a frozen anchor in the Physics De-Risking Register.

Explore the whole programme: the De-Risking Register, the interactive 3-D model, and the physics validator.

KRONOS FUSION ENERGY

A Real-Time Tritium-Accountancy Twin for a Compact Spherical-Tokamak Breeder: In-Vessel Inventory, Retention, and Self-Sufficiency Bookkeeping

A real fusion company building real machines. Explore the science, live.

Zenodo · doi:10.5281/zenodo.22645876

Read on kronosfusionenergy.com

The Physics De-Risking Register